

Thermal flywheel effects on the time varying conduction heat transfer through structural walls

P.T. Tsilingiris

*Department of Energy Engineering, Technological Education Institution (TEI) of Athens,
A. Spyridonos Street GR 122 10, Egaleo, Athens, Greece*

Received 30 March 2003; received in revised form 3 May 2003; accepted 3 May 2003

Abstract

Wall time varying conduction heat transfer investigations are very important for the prediction of heating and cooling loads in air conditioning practice and absolutely essential to the passive solar heating design. The walls store heat, absorb and dissipate a fraction of it and transmit the rest into the conditioned space at a later time, which depends on the wall thermal inertia. The present work aims at the description of a developed numerical model, which is validated successfully against analytical results from the literature and allows the prediction of transient and quasi-steady-state thermal behaviour of two basic structural wall design groups of a growing thermal inertia. The model allows the calculation of the time varying conduction heat flux for a wide range of progressively heavier wall designs, under the effect of time varying meteorological conditions, something which allows their design evaluation for a specific application. A drastic reduction of the daily fluctuation of the quasi-steady-state heat flux would be possible by using a broad range of heavier walls, something which can be quantified by the introduction of a dimensionless quantity defined as wall damping-out efficiency. This is attributed to the thermal inertia of a specific wall design, which is also responsible for phasing-out of the maximum heat flux. Both phenomena, which are comparatively investigated for the two groups of specified walls, are desirable particularly for the development of peak load control strategies.

© 2003 Elsevier B.V. All rights reserved.

Keywords: Thermal flywheel effect; Time varying conduction; Wall heat transfer

1. Introduction

The rapid expansion of climatic control technology in the contemporary human society is associated with the growing level of living standards world-wide. The use of all-year round air conditioning systems is widely spread over a broad range of human activities. The strongly time varying meteorological conditions and particularly the incident solar radiation and ambient temperature which are considered as important driving functions in climatic control systems influence considerably the level of air conditioning load in buildings. Neglecting the gain from internal heat generation sources, this load can be seen as the contribution of three main components. The first is the solar radiation transmitted by glass known as direct heat gain, while the second is the energy required to heat the infiltrated ambient air, known as infiltration and ventilation gain. The third component corresponds to the conduction heat transfer through the outer shell of the conditioned space. Among these, the first two occur simultaneously with the meteorological driving functions. Conduction heat transfer to the space, however, may

considerably lag the maximum rate of radiation absorption at the outer shell of the structure. Furthermore, owing to dissipation and absorption of heat at the outer building envelope, the maximum rate of heat conduction becomes a fraction of the maximum heat input at the external wall surfaces. The walls store and dissipate a significant fraction of heat and transmit the rest of it in the room after a time period, which is proportional to the heat storage capability of the room envelope. When all the three load components are in phase, the peak load may become excessively high, something which may impose the selection of over-size mechanical equipment of significant capital and operational costs, since the system is usually designed to meet the peak load. A significant reduction of the maximum load is possible by damping and phasing-out the wall conduction heat flux, using heavier structural elements of substantial thermal inertia. Any effort towards this aim may possibly lead to the reduction of peak load, system capacity and cost of climatic control equipment. Additional economic and social benefits would possibly be available due to the reduction of the peak power demand which is attributed to the use of air conditioning systems.

Nomenclature

a	total hemispherical absorptivity
A	numerical constant
Bi	Biot number
c	specific heat capacity (J/(kg K))
f	damping-out efficiency
Fo	Fourier number
h	convective heat transfer coefficient (W/(m ² K))
I	incident solar radiation (W/m ²)
k	thermal conductivity (W/(m K))
L	wall thickness (m)
q	heat flux rate (W/m ²)
t	time (s)
T	temperature (°C)
T^*	period (s)
ΔT	time lag (h)
x	space co-ordinate (m)

Greek letters

α	thermal diffusivity (m ² /s)
δ	layer thickness (m)
λ	numerical constant
ρ	density (kg/m ³)
ω	angular velocity (s ⁻¹)

Subscripts

a	amplitude
av	average
b	brick
c	concrete
ci	convective, indoor surface
c ∞	convective, outdoor surface
e	thermal insulation
i	indoor, initial
m	maximum
o	deviation from average
p	plaster
R	room
ri	radiative, indoor surface
r ∞	radiative, outdoor surface
s	summer
w	winter
∞	ambient

The whole strategy represents significant demand-side management advantages owing to the maximum power generating capacity thread, that most of the generating utilities confront, especially in the summer early evening hours due to excessively high air conditioning loads.

The use of massive walls of large thermal inertia aiming at the reduction of room temperature fluctuations in structures is not new. The problem was previously investigated by Maloney et al. [3], Duffin and Knowles [1,2], as well as by

Athienitis et al. [4], employing equivalent electrical network approaches. In these investigations, structural walls and meteorological driving functions are replaced by a combination of electrical elements as well as voltage and current sources, aiming to derive the time varying heat fluxes and calculate the temperature fluctuations in direct gain spaces. The present analysis is somewhat different in terms of purpose and approach. A simple and flexible transient heat transfer computer simulation model was developed, which allows the calculation of the wall time varying conduction heat transfer rate under the combined effect of time varying solar insolation and ambient temperature under specified room conditions for a wide range of practical wall designs. The transient and quasi-steady-state temperature fields and heat fluxes are calculated and the effect of a progressively increasing wall thermal inertia on the load control is investigated.

2. The development of the theoretical model

The heat flow in a plane wall of large lateral dimensions at direction perpendicular to the wall surface is governed by the one-dimensional conduction heat transfer equation:

$$\frac{\partial}{\partial x} \left(k \frac{\partial T}{\partial x} \right) = \rho c \frac{\partial T}{\partial t} \quad (1)$$

Assuming that the co-ordinate system is located at the external wall surface of a thickness L , separating a space at an indoor temperature $T_i(t)$ and the environment at the temperature $T_\infty(t)$, the boundary conditions of the equation are expressed in terms of the temperature gradient at the wall surfaces:

$$q(0, t) = -k \left(\frac{\partial T}{\partial x} \right) \Big|_{x=0} = aI(t) + (h_{co} + h_{ro})[T_\infty(t) - T(0, t)] \quad (2)$$

and

$$q(L, t) = -k \left(\frac{\partial T}{\partial x} \right) \Big|_{x=L} = (h_{ci} + h_{ri})[T(L, t) - T_i(t)] \quad (3)$$

where h_{co} , h_{ci} and h_{ri} , h_{ro} are the convective and radiative heat transfer coefficients for both the ambient and room wall sides, respectively, and a the wall total hemispherical absorptivity. For practical multiple layer walls, the thermophysical properties k , ρ and c are allowed to vary with the co-ordinate x .

Although the analytical approach of the problem, at least as far as the simple case of a solid medium with uniform thermophysical properties is concerned is possible [5], analytical solutions involving usually infinite series are difficult to obtain as well as inconvenient and time consuming to manipulate. It is broadly believed that numerical solutions and more specifically the treatment based on the finite difference method, which are easily adapted to the micro-computer technology, constitute a very powerful and flexible tool for the solution of such problems under highly refined boundary and initial conditions.

For the development of the finite difference model, the wall was subdivided into several uniform temperature and thermophysical property sublayer sections, at the centre of which a node of a thermal network was located. As soon as an initial condition was specified, a system of simultaneous algebraic equations was then developed by translating the differential equation (1) and the boundary conditions (2) and (3) into a set of simultaneous algebraic equations, corresponding to each inner and boundary nodes, using the always inherently stable Laasonen implicit finite difference scheme [6–8]. Derived results from alternative calculations using the same space and time intervals and the Crank–Nicholson approximation were always found to be practically identical.

The number of the simultaneous equations is equal to the thermal network nodes. The specified time domain is also subdivided into a large number of time steps and the solution of the set of simultaneous equations is carried out repeatedly throughout the whole number of integration time steps. The accuracy of calculations is proportional to the number of sublayer sections and integration steps, although their excessive increase may possibly lead to prohibitively lengthy computer simulation runs and large computer CPU time. The optimum selection of the wall sublayer number and time steps is a trade-off between CPU time and accuracy and was based on numerical experiments, which are discussed in greater detail by Tsilingiris [9]. The typical range of sublayer section thickness and time step was selected between 0.005 and 0.01 m, and 100 and 300 s, respectively.

The developed computer simulation code offers the flexibility of using any user defined time and space intervals and sets of various thermophysical properties for the sublayer materials. It also allows the incorporation of various user selectable initial and boundary conditions. For the purpose of the present investigation, the thermal radiation effects are assumed to be negligible as compared to the convective heat losses from both wall surfaces.

Referring to conditions in which the model simulates a conventional sunlit structural wall element, the variables $I(t)$ and $T_{\infty}(t)$ appearing in the expression (2) represent the periodic meteorological time-dependent forcing functions to the boundary conditions. Daily average, statistically treated incident solar radiation data for the Athens area were introduced in the model and a subroutine was developed for the calculation of the corresponding instantaneous data at the wall surface for any desired number of sequential days during the year, according to well established procedures [10,11]. Long-term daily range and average ambient temperature data were also employed to derive the appropriate time resolution ambient temperature time series for the desired sequence of simulation days, also based on standard procedures.

For the evaluation of the developed numerical model against the theory, analytical solutions of Eq. (1) in the form of infinite exponential series, representing the symmetric temperature distributions during the transient cooling of an infinite concrete slab, were derived from the relevant liter-

ature [12,13]. Since the exponential terms in the solutions converge rapidly with increasing time, it could be possible to maintain only the first term of the series without significant sacrifice of accuracy, under the assumption of dimensionless time Fourier numbers, $Fo = \alpha t/L^2 > 0.2$, where α is the thermal diffusivity of the medium and $L = 0.125$ m is now the half wall thickness. Neglecting all remaining terms leads to negligible (lower than 2%) errors, an assumption which constitutes the basis for the development of simplified solutions, the graphical presentation of which are known in the literature as Heisler charts [14]. When the slab at an initial temperature T_i is immersed at $t = 0$ in a fluid of a fixed ambient temperature T_{∞} , the transient temperature distributions according to this analysis are offered by the expression:

$$\frac{T(x, t) - T_{\infty}}{T_i - T_{\infty}} = A_1 \exp(-\lambda_1^2 Fo) \cos\left(\lambda_1 \frac{x}{L}\right) \quad (4)$$

The so calculated analytical solutions are strictly valid for Fourier number, $Fo = \alpha t/L^2 > 0.2$. It is assumed, that a slab at an initial temperature of $T_i = 60^\circ\text{C}$ is subjected to cooling at an environment of a constant temperature $T_{\infty} = 0^\circ\text{C}$ with $h = 20 \text{ W}/(\text{m}^2 \text{ K})$. The slab is characterized by uniform properties of $\rho = 2300 \text{ kg}/\text{m}^3$, $c = 880 \text{ J}/(\text{kg K})$ and $k = 1.4 \text{ W}/(\text{m K})$. The numerical constants A_1 and λ_1 are functions of the dimensionless Biot number, $Bi = hL/k$. For the derivation of comparative results from the present analysis, the computer model was slightly modified to accept the appropriate initial and boundary conditions, as well as to

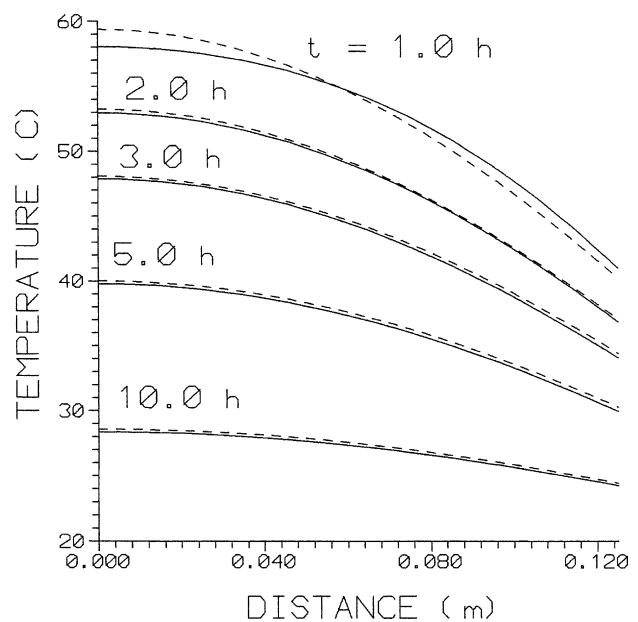


Fig. 1. Calculated comparative temperature profiles for $t = 1.0, 2.0, 3.0, 5.0$ and 10h according to the single exponential term analytical solution (broken lines) and to the developed numerical model (solid lines). Close agreement between results from analytical and numerical models is observed. The discrepancies for the $t = 1.0\text{h}$ profile, corresponding to a $Fo = 0.159$, are attributed to the errors associated to the single exponential term analytical solution in Eq. (4), which is strictly valid for $Fo > 0.2$.

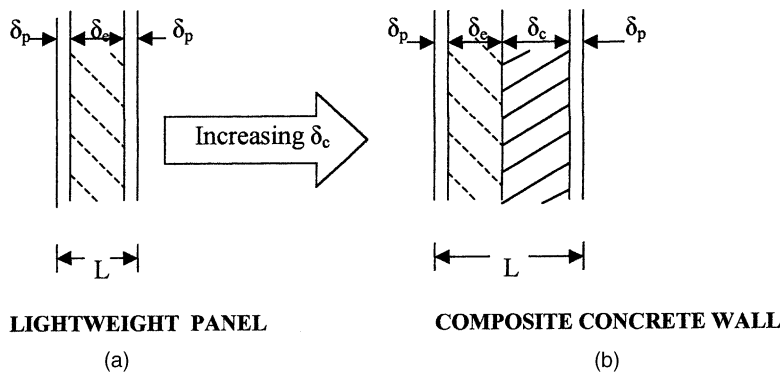
refer to a solid medium of uniform properties. Comparative results are shown in Fig. 1 in which the transient temperature profiles for fixed time intervals of 1.0, 2.0, 3.0, 5.0 and 10.0 h are shown during the process. Solid and broken lines correspond to numerical and analytical results, respectively. Apparently there is a remarkable agreement between both results for the temperature distributions at 2.0, 3.0, 5.0 and 10.0 h, corresponding to Fourier numbers of 0.318, 0.477, 0.796 and 1.592, respectively. For the first profile of $t = 1.0$ h and $Fo = 0.159$, significant discrepancies are observed which are attributed to the limitation of the analytical solution in (4), which is strictly valid only for $Fo > 0.20$, while the corresponding $Fo = \alpha t / L^2$ for the current conditions and $t = 1.0$ h is remarkably lower, $Fo = 0.1592 < 0.2$.

3. Description of the wall designs

A variety of wall designs are employed in the building industry, depending on the purpose and specific applica-

tion. They usually consist of successive layers of various materials, the thermophysical properties and geometry of which determine their thermal resistance and heat capacity. The increase of both these physical quantities leads to the reduction of the conduction heat losses and the corresponding increase of the wall thermal inertia, respectively, effects which strongly determine their transient thermal behaviour. Lightweight panels are basic walls, which as shown in Fig. 2a, are typically composed by a thermal insulation layer of a thickness δ_e , sandwiched between two plaster layers of a thickness δ_p . Although the heat capacity of this wall is relatively low, its thermal resistance can be appreciably high, depending on the thickness and thermal conductivity of the insulation layer. Heavier reinforced concrete or brick walls are more frequently employed in building construction practice, especially when they are destined as building support elements. A typical design of the reinforced concrete wall group is shown in Fig. 2b, in which a reinforced concrete slab of a thickness δ_c , thermally insulated by a layer of a thickness δ_e , is plastered at both sides with plaster layers of a thickness δ_p .

CONCRETE WALLS



BRICK WALLS

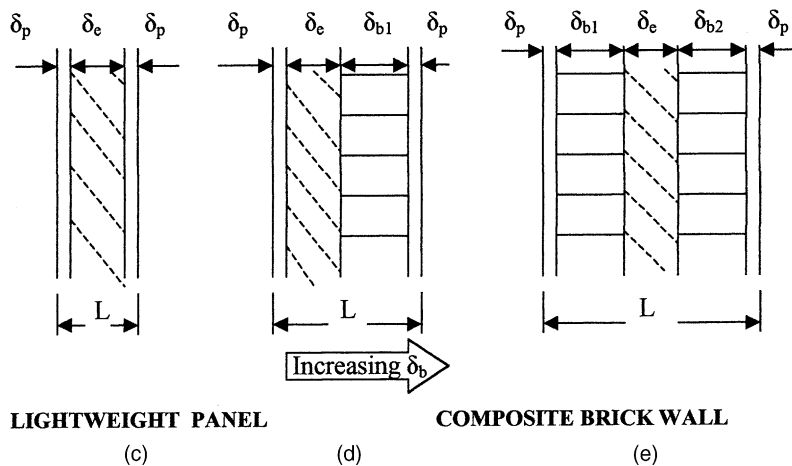


Fig. 2. Brief description of the investigated wall designs. Progressively heavier composite concrete or brick walls as shown in (b) or (d) and (e), respectively, are developed when concrete or brick layers of growing thickness δ_c or δ_{b1} and δ_{b2} , respectively, are included in the lightweight panel walls (a) and (c).

Table 1
Brief description of wall designs

	WC1	WC2	WC3	WC4	WC5	WC6
(1) Concrete walls						
δ_c (m)	0	0.10	0.20	0.30	0.40	0.50
L (m)	0.08	0.18	0.28	0.38	0.48	0.58
	WB1	WB2	WB3	WB4	WB5	WB6
(2) Brick walls						
δ_{b1} (m)	0	0.09	0.09	0.18	0.18	0.24
δ_{b2} (m)	0	0	0.09	0.06	0.18	0.24
δ_b (m)	0	0.09	0.18	0.24	0.36	0.48
L (m)	0.08	0.17	0.26	0.32	0.44	0.56

$\delta_p = 0.02$ m; $\rho_p = 2000$ kg/m³; $k_p = 1.39$ W/(m K); $c_p = 1085$ J/(kg K);
 $\delta_e = 0.04$ m; $\rho_e = 40$ kg/m³; $k_e = 0.041$ W/(m K); $c_e = 840$ J/(kg K);
 $\rho_c = 2300$ kg/m³; $k_c = 1.40$ W/(m K); $c_c = 880$ J/(kg K).

A wide range of single or double row brick wall designs may also be developed, the thickness of each row being usually a multiple of the standard brick width. Typical single and double brick layer walls are shown in Fig. 2d and e, respectively. In principle the single brick layer wall design is derived from the lightweight panel design when a single brick row layer of a thickness $\delta_b = \delta_{b1}$, is installed between the thermal insulation and plaster layers. In the double brick row wall design, two brick layers of thicknesses, δ_{b1} and δ_{b2} are placed symmetrically to the thermal insulation and the system is layered at both sides with plaster. The overall brick layer thickness of this wall is assumed to be $\delta_b = \delta_{b1} + \delta_{b2}$.

For the purpose of the present analysis, a wide range of concrete and brick wall designs was investigated, as shown in Fig. 2. A brief description of wall layer thicknesses and thermophysical properties are shown in Table 1. The range of the investigated concrete wall types WC2 to WC6 of $L = 0.17$ – 0.58 m as shown in Fig. 2a and b, were originally developed from the lightweight panel design wall WC1 of $\delta_c = 0$, by a progressive increase of δ_c between 0.1 and 0.5 m. The corresponding range of brick walls WB2 to WB6 with $L = 0.18$ – 0.56 m was also developed from the wall design type WB1 of $\delta_c = 0$ by a progressive increase of δ_b between 0 and 0.48 m, as also shown in Fig. 2c–e.

It can be seen that the concrete and brick layer thicknesses δ_c and δ_b , respectively, are allowed to vary between $\delta_c = \delta_b = 0$ m and $\delta_c = 0.5$ m and $\delta_b = 0.48$ m, respectively, corresponding to very massive concrete and double row brick wall structures WC6 and WB6 with widths $L = 0.58$ and 0.56 m, respectively. Assuming that δ_c and δ_b are the main wall design parameters, the thermal resistance and heat capacity of the investigated walls WC1 to WC6 and WB1 to WB6, is proportional to the concrete and the brick layer thickness, respectively. Therefore, reduction of δ_c and δ_b leads to the corresponding reduction of these physical quantities, which for $\delta_c = \delta_b = 0$ m are becoming identical to those of the lightweight panel type.

4. Results and discussion

For the purpose of the present analysis, the transient and quasi-steady-state thermal behaviour of the two groups of the walls WC1 to WC6 and WB1 to WB6 was investigated, under the combined effect of time varying typical meteorological forcing functions. The meteorological conditions correspond to Athens area, representing a typical mild Mediterranean climate. The 20th day of January and July as well as $T_i = 20$ and 26 °C were selected to be the first simulation day and the constant room temperatures, respectively, for winter and summer conditions.

The fixed total hemispherical absorption coefficient of the sunlit wall surface, which is assumed to be light painted, is $a = 0.2$. As initial condition the uniform temperature distribution of 10 and 30 °C was assumed for the winter and summer conditions, respectively.

From a number of preliminary simulations, it was found that the solution of the conduction heat transfer equation under the effect of time varying ambient temperature and incident solar radiation, leads to the development of transient temperature fields and corresponding heat fluxes, which asymptotically converge to their periodically time varying values. This occurs when all transients have died away and the transient being proportional to the wall heat capacity, lasts typically around 50 h. The time varying heat flux which corresponds to room heat gain or loss, $q(L, t)$ is calculated by expression (3). The simulations were carried out for a time domain of 120 h, corresponding to a sequence of five summer or winter days.

At quasi-steady-state conditions, the combined effect of the harmonically varying ambient temperature and time varying incident solar radiation causes the development of a periodically time varying heat flux function, $q(t) = q(t + T^*)$ with a period of $T^* = 24$ h. This function can be expressed in the form of infinite Fourier series:

$$q(t) = q_{av} + \sum_{n=1}^{\infty} [q_{1,n} \cos(n\omega t) + q_{2,n} \sin(n\omega t)] \quad (5)$$

where, $\omega = 2\pi/T^*$ is the angular velocity and

$$q_{av} = \frac{1}{T} \int_t^{t+T^*} q(t) dt \quad (6)$$

is the average heat flux and $q_{1,n}$, $q_{2,n}$ the Fourier coefficients:

$$q_{1,n} = \frac{2}{T} \int_t^{t+T^*} q(t) \cos(n\omega t) dt \quad (7)$$

$$q_{2,n} = \frac{2}{T} \int_t^{t+T^*} q(t) \sin(n\omega t) dt \quad (8)$$

4.1. The results for winter and summer simulations

Typical simulation results are plotted for winter conditions in Fig. 3. In this plot, the time varying heat fluxes for the concrete walls WC1 to WC6 were comparatively plotted

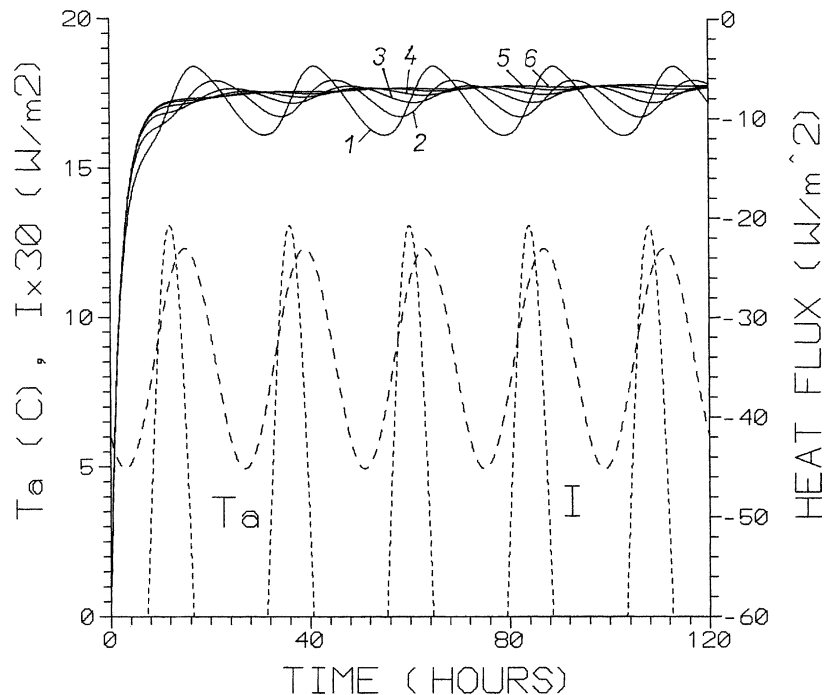


Fig. 3. Comparative presentation of the calculated heat fluxes for the lightweight panel WC1 (solid line 1) and the progressively heavier concrete walls WC2 to WC6 (solid lines 2–6), for a succession of five sequential winter days. In the same plot, the harmonically varying ambient temperature and the time varying solar insolation are also shown with broken and dotted lines, respectively.

by the corresponding solid lines 1–6. The negative sign in the calculated heat loss rates signifies the direction of the heat flow. The incident solar radiation at a south oriented vertical wall was also plotted in dotted line along with the harmonically varying ambient temperature, which is also shown in broken line.

It can be seen that during the first simulation steps, remarkably high transient heat loss rates, as high as 56 W/m^2 occur, irrespectively of the wall thickness. These are rapidly decreasing, converging to the periodic solution values. This practically occurs between about 40 and 70 h depending on the wall thickness which determines its thermal inertia.

The average value of the periodically time varying heat flux q_{av} depends on various parameters, among which the incident solar radiation, the absorption coefficient of the wall surface, the average value of the ambient temperature and the wall thermal resistance dominates. It is calculated for the fifth simulation day by the following expression for $t_1 = 96 \text{ h}$ and $t_2 = 120 \text{ h}$:

$$q_{av} = \frac{1}{t_2 - t_1} \int_{t_1}^{t_2} q(t) dt \quad (9)$$

This quantity decreases from the value of -8.403 W/m^2 corresponding to the wall WC1 to the value of -6.697 W/m^2 corresponding to the wall WC6. This is due to the respective reduction of the wall thermal resistance, which is attributed to the increase of the concrete layer thickness from $\delta_c = 0$ to 0.5 m .

According to the derived results, the time varying heat flux $q(t)$ fluctuates around its average quasi-steady-state value. The maximum heat flux deviation from its average value overnight is higher than the corresponding value during the day, owing to the combined effect of radiation absorption at the outer wall surface and ambient temperature. This leads to a maximum wall heat flux during the early morning hours of the day. As can be seen from the same plot, the difference between the daily maximum and minimum heat flux, which represents the daily maximum heat flux swing, is inversely proportional to the wall thickness. As derived from Fig. 3, it decreases from about 7.72 W/m^2 to the almost negligible value of 0.05 W/m^2 as the wall thickness increases from $L = 0.08$ to 0.58 m corresponding to wall types WC1 and WC6, respectively. It is also remarkable to note the increasing phase lag Δt between the developed maximum value of time varying heat flux and the maximum ambient temperature, which indicates the peak load phasing-out wall efficiency, as the thickness increases and the wall becomes heavier.

The corresponding results for the second group of brick walls are shown in Fig. 4. In this plot the time varying heat fluxes for the walls WB2 to WB6 of $L = 0.17$ – 0.56 m , respectively, were comparatively plotted to the corresponding heat flux for the wall WB1 with $L = 0.08 \text{ m}$ in solid lines. In the same plot, the incident solar radiation and ambient temperature were also plotted in dotted and broken lines, respectively.

As with the group of concrete walls, remarkably high heat loss rates occur during the first simulation steps

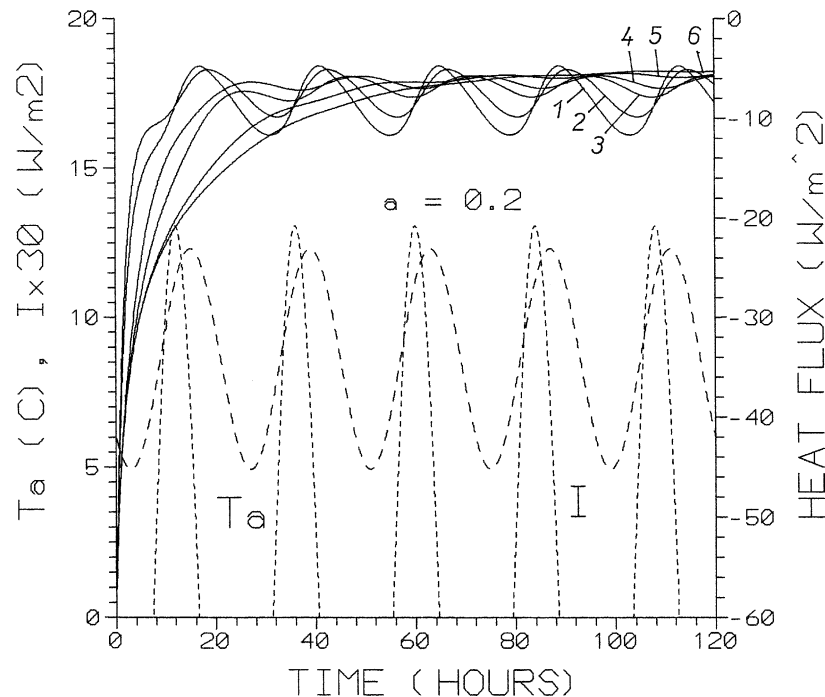


Fig. 4. Comparative presentation of the calculated heat fluxes for the lightweight panel WB1 (solid line 1) and the progressively heavier brick walls WB2 to WB6 (solid lines 2–6), for a succession of five sequential winter days. In the same plot, the harmonically varying ambient temperature and the time varying solar insolation are also shown with broken and dotted lines, respectively.

irrespectively of the wall thickness. These transient heat loss rates are rapidly decreasing and the solutions converge asymptotically to their periodic values, between about 40 and 90 h depending on the wall thickness.

The average value of the periodically time varying heat flux decreases now from the value of -8.403 W/m^2 to the value of -5.353 W/m^2 corresponding to the walls WB1 to WB6, respectively. This is attributed to the reduction of the wall thermal resistance, owing to the corresponding increase of the brick layer thickness from $\delta_b = 0$ to 0.48 m , which is more rapid as compared to concrete walls, owing to the lower thermal conductivity of brick layers. A decrease of the calculated daily maximum quasi-steady-state heat flux swing and a corresponding increase of phase lag Δt between the developed maximum value of the time varying heat loss rate and the maximum ambient temperature can also clearly be seen, as the wall width increases from $L = 0.08$ to 0.56 m corresponding to the walls WB1 to WB6, respectively.

The corresponding simulation results for the summer conditions are shown in Figs. 5 and 6 for the entire range of concrete and brick walls, respectively. Due to the specified initial conditions of the problem, significant transient heat flux rates as high as 33 W/m^2 , irrespectively of the specific wall design occur during the first simulation steps. The transient, depending as previously on the specific wall design, lasts about 80 h before quasi-steady-state conditions are established with the exception of the heavier brick walls, for which it lasts even longer.

4.2. Effects and implications on the load time dependence

According to the derived results, it is obvious that for summer conditions, at least as far as the walls WC1 to WC3 and WB1 to WB3 is concerned, the calculated quasi-steady-state heat flux becomes alternatively positive (heat gain) and negative (heat loss). This is attributed to the combined effect of the time varying incident solar radiation and the harmonically varying ambient temperature, which becomes daily for a certain period of time, lower than room temperature. This causes a time varying heat flux of significant daily maximum swing although of a small average value. As the concrete or brick layer thickness increases, it causes a corresponding increase of wall thermal resistance and heat capacity. This results to a decrease of the average heat flux as well as to a significant damping-out effect of the daily maximum heat flux deviation, which leads to always positive heat flux corresponding to heat gain.

It is important to note that the calculated average heat loss rate during quasi-steady-state conditions for summer is smaller than the corresponding quantity during winter. This is mainly attributed to the smaller difference between room and average ambient temperature, as well as to the higher level of the incident solar radiation at the outer wall surface during the summer. Also, the calculated daily maximum heat flux swing for summer is comparably higher than for winter conditions, owing to the appreciably higher level (about

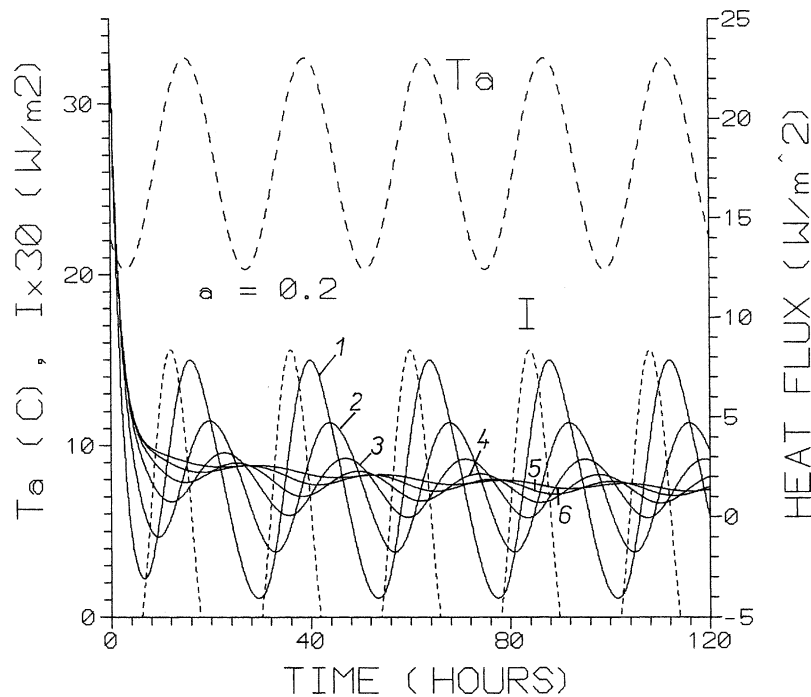


Fig. 5. Comparative presentation of the calculated heat fluxes for the lightweight panel WC1 (solid line 1) and the progressively heavier concrete walls WC2 to WC6 (solid lines 2–6), for a succession of five sequential summer days. In the same plot, the harmonically varying ambient temperature and the time varying solar insolation are also shown with broken and dotted lines, respectively.

35%) of incident solar radiation at the wall surface during summer.

The maximum heat flux q_m , which strongly contributes to the peak load of an air conditioned space, is an important

design parameter in air conditioning load calculations. This quantity for a wall of a concrete layer thickness δ_c or a brick layer thickness δ_b is expressed as:

$$q_m(\delta_c) = q_{av}(\delta_c) + q_o(\delta_c) \tag{10}$$

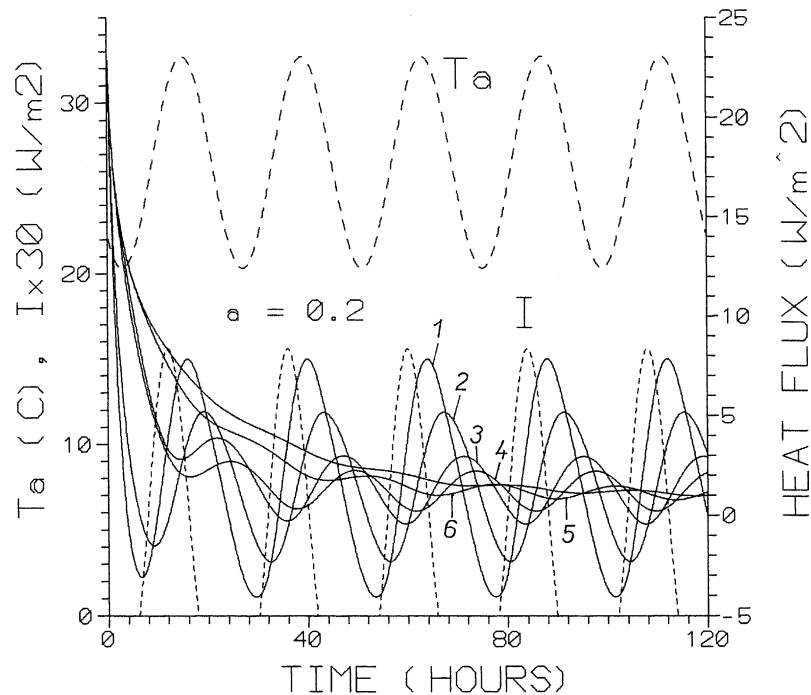


Fig. 6. Comparative presentation of the calculated heat fluxes for the lightweight panel WB1 (solid line 1) and the progressively heavier brick walls WB2 to WB6 (solid lines 2–6), for a succession of five sequential summer days. In the same plot, the harmonically varying ambient temperature and the time varying solar insolation are also shown with broken and dotted lines, respectively.

and

$$q_m(\delta_b) = q_{av}(\delta_b) + q_o(\delta_b) \tag{11}$$

where q_o is the heat flux deviation from its average value. While the same quantity for a lightweight panel is $q_m(\delta_c = 0) = q_m(\delta_b = 0)$, any effort towards reducing or phasing-out the wall conduction heat flux is highly desirable. Proper wall design may strongly contribute towards this aim. The results of the present analysis indicates that the use of massive walls contributes towards the strong damping and phasing-out of conduction heat flux. As damping-out efficiency of concrete walls for winter and summer conditions, $f_{c,w}$ and $f_{c,s}$, the following dimensionless quantities are defined as:

$$f_{c,w} = \left| \frac{q_m(\delta_c)}{q_m(\delta_c = 0)} \right|_w \tag{12}$$

and

$$f_{c,s} = \left| \frac{q_m(\delta_c)}{q_m(\delta_c = 0)} \right|_s \tag{13}$$

The respective quantities for brick walls are:

$$f_{b,w} = \left| \frac{q_m(\delta_b)}{q_m(\delta_b = 0)} \right|_w \tag{14}$$

and

$$f_{b,s} = \left| \frac{q_m(\delta_b)}{q_m(\delta_b = 0)} \right|_s \tag{15}$$

respectively. These dimensionless quantities represent the heat flux damping-out efficiency for winter or summer of a

particular wall, as the concrete or the brick layer increases and the wall becomes heavier.

In Figs. 7 and 8, the dimensionless quantities $f_{c,w}$, $f_{c,s}$ and $f_{b,w}$, $f_{b,s}$, the absolute value of the average heat flux q_{av} and the time lag Δt in hours between the maximum ambient temperature and the peak quasi-steady-state heat flux were comparatively plotted as a function of the wall thickness L , for the reinforced concrete and the brick walls, respectively.

In Fig. 7, the three pairs of solid, broken and dotted fit lines represent the damping-out efficiency f , the average heat loss q_{av} and the time lag Δt , respectively, which are plotted against the wall thickness for the concrete walls WC1 to WC6 corresponding to $L = 0.08$ – 0.58 m. The large data point symbols of the first of each pair of lines correspond to the winter, while the similar smaller symbols to the summer conditions. It can clearly be seen that f decreases sharply as the concrete wall thickness increases, something which leads to a significant reduction of the peak wall heat flux. For massive walls similar to WC6, the dimensionless quantities $f_{c,s}$ and $f_{c,w}$ are estimated to be as high as 0.212 and 0.578 for summer and winter conditions, respectively. The significantly slower decrease of this parameter for winter conditions is attributed to the corresponding slower reduction of amplitude and average wall heat flux, as derived from Figs. 3 and 5.

In the same figure, the average quasi-steady-state heat loss rate data points are shown, fitted in broken straight lines. The slope of these lines for summer and winter conditions is -0.343 and -0.036 W/m^3 , respectively. The negative slope

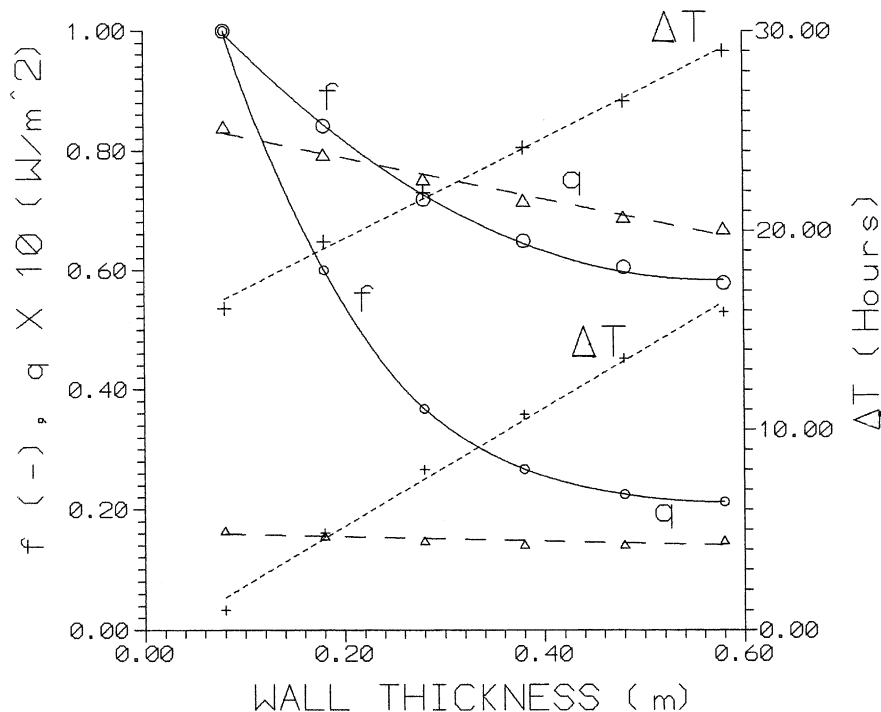


Fig. 7. Comparative plot of average heat flux, damping-out efficiency and time lag in hours for the concrete walls. The large discrete data points correspond with winter while the smaller with summer conditions. The average heat flux fit line is plotted in broken line while the phasing-out time lag Δt in hours is plotted in dotted lines. The damping-out efficiencies $f_{c,w}$ and $f_{c,s}$ are plotted in solid lines.

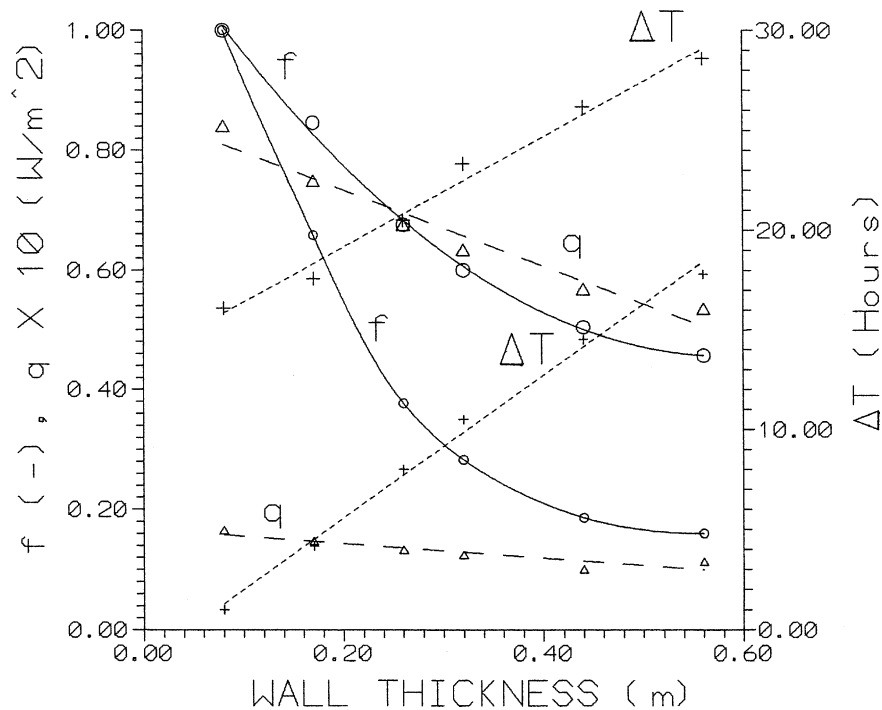


Fig. 8. Comparative plot of average heat flux, damping-out efficiency and time lag in hours for the brick walls. The large discrete data points correspond with winter while the smaller with summer conditions. The average heat flux fit line is plotted in broken line while the phasing-out time lag Δt in hours is plotted in dotted lines. The damping-out efficiencies $f_{b,w}$ and $f_{b,s}$ are plotted in solid lines.

is attributed to the increase of wall thermal resistance with the concrete layer thickness. The slope of the data fit line for the winter is higher than for summer conditions, mainly owing to the higher difference between room and daily average ambient temperature, although even higher slopes should be expected. This is due to the higher than expected numerical values for the wall WC6, which is attributed to its unusually heavy design, leading to an excessively long transient before the development of quasi-steady-state conditions.

Finally, the data points corresponding to the time lag between maximum ambient temperature and peak wall heat flux are shown, fitted in dotted straight lines for summer and winter conditions. The time lag for winter conditions and the walls WC1 to WC6 ranges from about 16 to 29 h, owing to the fact that maximum heat losses occur during early morning hours when ambient temperatures are minimum. The corresponding time lag for summer conditions, ranges between about 1 and 15.9 h. This is attributed to the fact that although the maximum wall heat gain during summer is almost in phase with maximum ambient temperature for the wall WC1, the phasing-out effect of the heavier concrete walls WC2 to WC6 is significant, shifting the peak wall heat flux up to about 15 h as the concrete layer thickness increases up to 0.5 m.

The corresponding results for the brick walls are shown in Fig. 8. The qualitatively similar behaviour of the quantity f leads to even lower numerical values for $f_{b,s}$ and $f_{b,w}$ for the heavier wall WB6, around to 0.160 and 0.457

for summer and winter conditions, respectively, something which suggests even better damping-out efficiency of brick walls. In the same plot, the steeper slope of the average quasi-steady-state wall heat flux fit lines is attributed to the lower thermal conductivity of the brick layers, which leads to more rapid increase of the wall thermal resistance. Finally, as before the time lag for the walls WB1 to WB6 ranges from about 16 to 28.5 h and from about 1 to 17.8 h for winter and summer conditions, respectively.

5. Conclusions

The accurate prediction of time varying conduction heat transfer which strongly influences the air conditioning load, is vital since it may considerably lag the direct heat gain load components which occur in phase with ambient temperature and solar radiation incident at the outer building envelope. This is due to the thermal flywheel effects, which become stronger as the structural wall elements become heavier. This effect is responsible for the reduction and phasing-out the peak load, which is strongly desirable in the climatic control system design. A numerical computer simulation model was developed, which allowed the prediction of the transient thermal behaviour and the time varying conduction heat flux for a wide range of practical, progressively heavier composite concrete and brick structural walls, frequently employed in construction. The present model was successfully validated against theory, using analytical solutions reported previously

in the literature. Simulation results were presented and the time varying heat fluxes were calculated for typical weather corresponding to a mild Mediterranean climate for conditions corresponding to summer and winter operation. Comparative presentation of the derived results indicate that both design groups of concrete and brick walls of progressively increasing thickness exhibit a qualitative similar behaviour, being more efficient to damp-out during summer and phase-out during winter the maximum time varying conduction heat flux. Comparing the specific effects for a particular season of operation, brick walls although appearing to be far more superior in damping-out, they phase out almost comparably to the concrete walls during winter. Regarding summer conditions, brick walls appear to be almost equally capable to damp and phase-out slightly better than concrete walls.

References

- [1] R.J. Duffin, G. Knowles, A passive wall design to minimise building temperature swings, *Solar Energy* 33 (3/4) (1984) 337–342.
- [2] R.J. Duffin, G. Knowles, Use of layered walls to reduce building temperature swings, *Solar Energy* 33 (6) (1984) 543–549.
- [3] J. Maloney, T.-C. Wang, B. Chen, J. Thorp, Thermal network predictions of the daily temperature fluctuations in a direct gain room, *Solar Energy* 29 (3) (1982) 207–223.
- [4] A.K. Athieitis, H.F. Sullivan, K.G.T. Hollands, Analytical model, sensitivity analysis and algorithm for temperature swings in direct gain rooms, *Solar Energy* 36 (4) (1986) 303–312.
- [5] H.S. Carslaw, J.C. Jaeger, *Conduction of Heat in Solids*, Clarendon Press, Oxford, 1959.
- [6] R.D. Richtmeyer, *Difference Methods for Initial-Value Problems*, Interscience, New York, 1957.
- [7] D.R. Croft, D.G. Lilley, *Heat Transfer Calculations Using Finite Difference Equations*, Applied Science Publishers, London, 1977.
- [8] W.M. Rohsenow, I.P. Hourtnett, Y.I. Cho (Eds.), *Handbook of Heat Transfer*, McGraw-Hill, New York, 1973.
- [9] P.T. Tsilingiris, On the transient thermal behaviour of structural walls—the combined effect of time-varying solar radiation and ambient temperature, *Renewable Energy* 27 (2002) 319–336.
- [10] J.A. Duffie, W.A. Beckmann, *Solar Engineering of Thermal Processes*, Wiley, New York, 1980.
- [11] P.T. Tsilingiris, Solar water heating design—a new simplified dynamic approach, *Solar Energy* 57 (1) (1996) 19–28.
- [12] F.P. Incropera, D.P. DeWitt, *Fundamentals of Heat and Mass Transfer*, second ed., Wiley, New York, 1985.
- [13] Y.A. Cengel, *Heat Transfer*, McGraw-Hill, New York, 1998.
- [14] M.P. Heisler, Temperature charts for induction and constant temperature heating, *Transactions ASME* 69 (1947) 227–236.